Accepted for publication in the Journal of Composites for Construction, ASCE

Dilation Effects in FRP-confined Square Concrete Columns using Stone, Brick and Recycled Coarse Aggregates

M.M. Islam[1], M.S.I. Choudhury[2], A.F.M.S. Amin[3]
Department of Civil Engineering
Bangladesh University of Engineering and Technology, Dhaka 1000, Bangladesh

ABSTRACT

The axial capacity enhancement of square plain concrete columns due to fiber-reinforced polymer (FRP) wrap is measured through experiments as a function of the fundamental dilation property of the parent concrete. To this end, unconfined (control) and FRP-confined concrete column specimens made using stone, brick, recycled stone and recycled brick aggregates having their own dilation properties were subjected to uniaxial compression. The dilation effect measured using the digital image correlation technique (DICT) was observed to have a distinct relation with the concrete modulus of elasticity resulting from the coarse aggregate unit weight and absorption capacities. Relations between the strengthening ratio and strain enhancement ratio with the actual confinement ratio were plotted to measure the confinement effectiveness coefficients and strain enhancement coefficients using a redefined confining pressure model. The measured coefficients are found to be distinctly lower for brick and recycled aggregate concretes than for stone aggregate concrete. This confirms the necessity of using a revised set of coefficients to estimate the effective confinement in columns of aggregates that exhibit a greater dilation property in concrete.

Author keywords: Brick aggregate, recycled brick aggregate, stone aggregate, recycled stone aggregate, fiber-reinforced polymer (FRP), dilation; digital image correlation technique (DICT), square columns, confined concrete model.

INTRODUCTION

The recent garment factory building collapses in Bangladesh (c.f. Miller 2013 for 2005 Spectrum Sweater Factory collapse, Yardley 2013 for 2013 Rana Plaza collapse) have raised awareness of the necessity of strengthening existing factory buildings to achieve building safety compliance. In this context, structurally deficient columns, as one of the most critical members in a structure, are a major focus in strengthening noncompliant buildings. Confining the columns (c.f. Saadatmanesh et al. 1994; Mirmiran and Shahawy 1997a,b; Shahawy et al. 2000; Teng et. al. 2002; Lam and Teng 2003a,b) with fiber-reinforced polymer (FRP) is competitive with

[1] Graduate student
[2] Graduate student
[3]Corresponding author: Prof. Dr. A.F.M. Saiful Amin, Department of Civil Engineering, Bangladesh University of Engineering and Technology, Dhaka 1000, Bangladesh. Email: samin@ce.buet.ac.bd Fax: +880-2-9665639 Telephone: +880-2-9671155

conventional reinforced concrete jacketing. In the FRP confinement technique, installation is faster and the floor-space reduction is lesser than in the case of the reinforced concrete jacketing technique. Nevertheless, enhanced axial capacity, the desired result of FRP confinement, is only achieved when the core concrete dilates under axial compression and induces hoop strain in the installed FRP wrap. The magnitude of the concrete dilation under a given axial load depends largely on the fundamental Poisson effect of the parent concrete. Concrete columns with higher dilation due to lower modulus of elasticity should produce greater strain in FRP confinement, resulting in early rupture with lower axial capacity enhancement. The features originating from the concrete itself certainly require proper attention in confinement design.

In this context, the scenario of the conventional use of crushed stone as a coarse aggregate is different than the scenario where crushed brick is used as the coarse aggregate. Because of the acute scarcity of natural stones, the use of crushed brick as a coarse aggregate as an alternative to natural stones is very common in Bangladesh and some parts of India. Concretes of brick aggregate are characteristically of lower unit weight, higher porosity (indicated by their high absorption capacity) and, most importantly, lower modulus of elasticity (c.f. Akhtaruzzaman and Hasnat 1983; Mansur et. al. 1999; Khalaf and DeVenny 2005; Khalaf 2006; Debieb and Kenai 2008; Cachim 2009). Recycled stone and brick aggregates, which have been extensively studied as viable alternatives to natural stone aggregates, have similar characteristic properties (c.f. Buck 1977; Frondistou-Yannas 1977; Hansen and Narud 1983; Xiao et al. 2005; Yang et al. 2008; Mohammed et al. 2014). Nevertheless, such a reduction in the modulus of elasticity of the concrete (Figure 1) must have a direct impact on the respective Poisson effects, leading to their fundamental dilation property (see also Zhao et al. 2014 for FRP-confined recycled stone aggregate concrete, Wang and Wu 2008 for observations on the larger hoop strain in FRP-confinement in lower grades of concrete). This particular feature observed in these aggregates demands a thorough experimental characterization to reestablish the coefficients of the fundamental interrelations between f'_{cc}/f'_{co}, f_l/f'_{co} and $\varepsilon_{cu}/\varepsilon_{co}$, where f'_{cc}=confined compressive strength, f'_{co}=unconfined compressive strength of the parent concrete, $f_l = \frac{2 f_{frp} t_{frp}}{D} = \frac{2 E_{frp} \varepsilon_j t_{frp}}{D} =$ confining pressure due to the FRP wrap when it fails by rupture due to the hoop tensile stresses (i.e., the maximum confining pressure possible with the jacket), f_{frp} = tensile strength of the FRP wrap, t_{frp} = thickness of the FRP wrap, E_{frp} = modulus of elasticity of the FRP wrap; $\varepsilon_j = \varepsilon_{l,rup}$ = nominal hoop rupture strain of the FRP wrap; and D = equivalent column diameter (Lam and Teng 2003a). Figure 2 presents a schematic of the confinement effect in a noncircular column. The principal stress paths in a confined noncircular column converge toward the corners, keeping the column sides at lower stress levels (Lam and Teng 2003a). In such columns, the general relations (after Richart et al. 1928, 1929) can be re-written as follows:

$$\frac{f'_{cc}}{f'_{co}} = 1 + k_1 k_{s1} \frac{f_{lD}}{f'_{co}} \quad (1)$$

$$\frac{\varepsilon_{cu}}{\varepsilon_{co}} = 1 + k_2 k_{s2} \frac{f_{lD}}{f'_{co}} \quad (2)$$

where $k_1 =$ the confinement effectiveness coefficient, $k_2 =$ the strain enhancement coefficient, and k_{s1} and k_{s2} are the shape factors to obtain f'_{cc} in noncircular columns. By considering ε_{lD}, the lateral strain due to volumetric dilation (Issa et al. 2009; Mirmiran and Shahawy 1997a,b) at the failure location, as a measure of dilation (Figures 1 and 4; see also Wu and Wei 2010; Lam and Teng 2003a; Mirmiran et al. 1998; Lim and Ozbakkaloglu 2014), the expression of f_{lD} is redefined from the expression of f_l as

$$f_{lD} = \frac{2E_{frp}\varepsilon_{lD}t_{frp}}{D}\upsilon \tag{3}$$

where υ is a proportionality factor/function to incorporate a relation between $\varepsilon_j \left(= \varepsilon_{l,rup}\right)$ and ε_{lD}. In Figure 9 of their paper, Wu and Wei (2010) measured υ to be 1.00 up to appreciable loadings, particularly in square columns. Shehata et al. (2002), ACI 440.2R (2002), Teng et al. (2007), ACI 440.2R (2008), Girgin (2009), Wu and Wang (2009) and Toutanji et al. (2010) reviewed design-oriented models, more rigorous analysis-oriented models and various functions of their own to define k_{s1} and k_{s2} based on a test database of FRP-confined stone aggregate concrete columns. Table 1 lists a few typical confined concrete models. Nevertheless, there has been no attempt to estimate the parameters k_1k_{s1} and k_2k_{s2} for brick, recycled brick and recycled stone aggregate concretes to allow the designers to appropriately strengthen columns made of these aggregates.

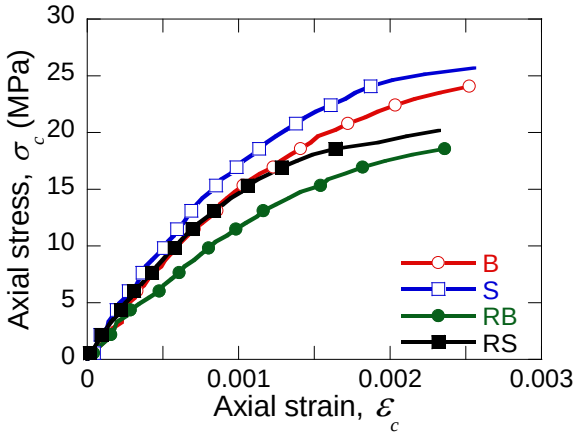

Fig. 1. Comparative stress-strain responses from plain concrete of different aggregates. S: Stone aggregate; B: Brick aggregate; RB: Recycled brick aggregate; RS: Recycled stone aggregate. Redrawn using the dataset taken from Mohammed et al. (2007). Values of the modulus of elasticity, E_c, for stone aggregate concrete, brick aggregate concrete, recycled stone aggregate concrete and recycled brick aggregate concrete (measured by the slopes of the responses at 0.0005 strain) are measured as 2.00 x 10^4, 1.74 x 10^4, 1.70 x 10^4, and 1.32 x 10^4 MPa, respectively, from this dataset.

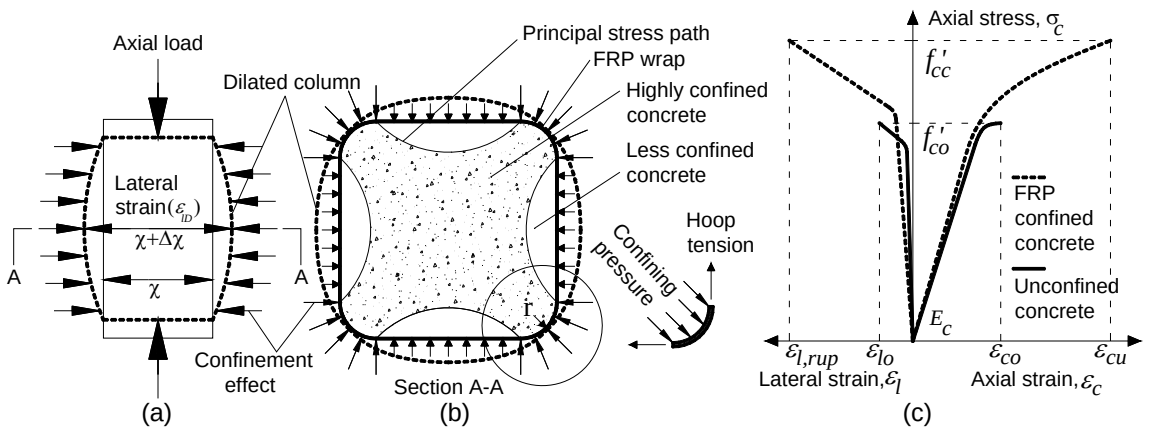

Fig. 2. Confining action of FRP in a square column (a) Dilation mechanism under axial load (b) confining pressure and dilation in an FRP-confined square concrete column (section A-A), arrows are scaled down at sides to indicate a reduced confinement and free-body diagram of the FRP wrap at the corner, rounded at a radius r to reduce the stress concentration as per ACI 440.2R (2008), see also Rochette and Labossière (2000), Wang and Wu (2008), and Wu and Wei (2010). (c) axial and lateral stress–strain behavior for an unconfined column with an ultimate axial strength f'_{co} and FRP-confined concrete column's ultimate axial strength, f'_{cc}, ε_{co}: ultimate compressive strain of an unconfined column, ε_{cu}: confined compressive strain, ε_{lo}: ultimate lateral strain at rupture of an unconfined column, $\varepsilon_{l,rup}$: ultimate lateral strain at rupture of a confined column, E_C: elastic modulus of an unconfined concrete. Lateral strain, $\varepsilon_{lD}\ (=\Delta\chi/\chi)$, is taken as an indirect measure of the dilation effect, where χ is the initial width of the column and $\Delta\chi$ is the increase in width due to dilation.

The measurement of local dilation in noncircular concrete columns under axial load demands special attention in adopting an appropriate experimental technique. In a non-uniform stress situation arising out of the specimen geometry and end conditions, the measurement of the hoop strain (circumferential strain), ε_r, using strain gauges attached on the wrap was used as an alternative to volumetric strain measurement (c.f. Mirmiran and Shahawy 1997a,b; Shahawy et al. 2000; Rochette and Labossière 2000; Pessiki et al. 2001; Lam and Teng 2003a; Smith et al. 2010; Luca et al. 2011; Zhao et al. 2014) to express the lateral strain, ε_{lD}. Wu and Wei (2010) compared strain gauge readings with lateral strain measurements obtained using a linear variable displacement transducer attached across the specimen. However, in a destructive test, there exists an obvious uncertainty in anticipating the failure location over the height of a short column. Furthermore, a concrete column, due to its inherent brittleness, undergoes an infinitesimal lateral strain over a short duration before initiating the brittle failure process. With the advent of high definition (HD) digital video cameras capable of capturing 60 or more frames per second, it is now possible to digitally capture the deformation history of the entire specimen throughout the test. In the digital image correlation technique (DICT), the time history of any strain component of interest at the failure location can be realized via a suitable image processing algorithm that post-processes recorded still image frames taken from the HD video footage and suitably correlates them with the applied loading history of the load cell to realize the load-displacement or stress-strain response. This technique was successfully followed by the authors in Islam (2011), Islam et al. (2011) and Choudhury (2012) for measuring the lateral strain in unconfined

and FRP-confined columns by employing a logical sequence to correlate the image history with load cell outputs. Recent comprehensive reviews on the adoption of DICT are available in El-Hacha and Abdelrahman (2013) and Abdelrahman and El-Hacha (2014a,b). However, detailed information on employing this technique to measure the confinement effectiveness of columns of different aggregate types has yet to be well-archived in the literature.

Table 1: Confined concrete models for noncircular plain concrete columns

References	Confined concrete models		
	Compressive strength models	Ultimate axial strain models	Confining pressure models
Shehata et al. (2002)	$\frac{f'_{cc}}{f'_{co}} = 1 + 0.85\left(\frac{f_l}{f'_{co}}\right)$	$\frac{\varepsilon_{cu}}{\varepsilon_{co}} = 1 + 13.5\left(\frac{f_l}{f'_{co}}\right)$	$f_l = \frac{2 f_{frp} t_{frp}}{D}$
Lam and Teng (2003a), see also Eqn. 2.	$\frac{f'_{cc}}{f'_{co}} = 1 + 3.3\left(\frac{A_e}{A_c}\right)\left(\frac{b}{h}\right)^2\left(\frac{f_l}{f'_{co}}\right)$	$\frac{\varepsilon_{cu}}{\varepsilon_{co}} = 1.75 + 12\left(\frac{h}{b}\right)^{0.5}\frac{f_l}{f'_{co}}\left(\frac{\varepsilon_{frp}}{\varepsilon_{co}}\right)^{0.45}$	$f_l = \frac{2E_{frp}\varepsilon_{frp}t_{frp}}{D}$
Al-Salloum (2007)	$\frac{f'_{cc}}{f'_{co}} = 1 + 3.14 k_e\left(\frac{b}{D}\right)\left(\frac{f_l}{f'_{co}}\right)$	-	$f_l = \frac{2 f_{frp} t_{frp} k_e}{D_1}$
Kumutha et al. (2007)	$\frac{f'_{cc}}{f'_{co}} = 1 + 0.93\left(\frac{f_l}{f'_{co}}\right)$	-	$f_l = \frac{2 f_{frp} t_{frp}}{D} = \frac{2 t_{frp} f_{frp}}{b}$
Youssef et al. (2007)	$\frac{f'_{cc}}{f'_{co}} = 0.5 + 1.225\left(\frac{k_{e1} f_l}{f'_{co}}\right)^{3/5}$	$\varepsilon_{cu} = \left[\lambda + 0.26\left(\frac{k_{e1} f_l}{f'_c}\right)\left(\frac{f_{frp}}{E_{frp}}\right)^{\frac{1}{2}}\right]$	$f_l = \frac{2 f_{frp} t_{frp} k_{e1}}{D}$
Wu and Wang (2009)	$\frac{f'_{cc}}{f'_{co}} = 1 + 2.23\left(2r/b\right)^{0.73}\left(\frac{f_l}{f'_{co}}\right)^{0.96}$	-	$f_l = \frac{2E_{frp}\varepsilon_{frp}t_{frp}}{b}$
ACI 440.2R (2002)	$\frac{f'_{cc}}{f'_{co}} = 2.25\sqrt{1 + 7.9\frac{f_l}{f'_c}} - 2\frac{f_l}{f'_c} - 1.25$	$\varepsilon_{cu} = \frac{1.71(5 f'_{cc} - 4 f'_{co})}{E_c}$	$f_l = \frac{\kappa_a \rho_f E_{frp} \varepsilon_{fe}}{2}$
ACI 440.2R (2008), see also Eqn. 2.	$\frac{f'_{cc}}{f'_{co}} = 1 + 3.3\psi_f\frac{A_e}{A_c}\left(\frac{b}{h}\right)^2\left(\frac{f_l}{f'_{co}}\right)$	$\varepsilon_{cu} = \varepsilon_{co}\left(1.5 + 12\frac{A_e}{A_c}\left(\frac{h}{b}\right)^{0.5}\frac{f_l}{f'_{co}}\left(\frac{\varepsilon_{frp}}{\varepsilon_{co}}\right)^{0.45}\right)$	$f_l = \frac{\sqrt{2}\psi_f E_{frp}\varepsilon_{frp}t_{frp}}{b}$

A_e: Effective confinement area; A_c: Concrete area; k_e and k_{e1}: Shape modification factor; defined in Al-Salloum (2007) and Youssef et al. (2007), respectively, for noncircular sections; the ACI reduction factor, ψ_f, is 0.95, λ: shape factor; defined in Youssef et al. (2007). In Lam and Teng (2003a) and ACI 440.2R (2008), the strain equation $\varepsilon_{l,rup}$ is replaced with ε_{frp}. ACI 440.2R 2002 defines $f_l = \kappa_a \rho_f E_{frp} \varepsilon_{fe}/2$ where, $\kappa_a = 1 - (b-2r)^2 + (h-2r)^2/3bh(1-\rho_g)$ and $\rho_f = 4t_{frp}/b$; $D_1 = \sqrt{2}b - 2r(\sqrt{2}-1)$, as used by Al-Salloum (2007); $\rho_{frp} = 2(b+h)t/bh$ is used in Kumutha et al. (2007). The effective confinement area ratio A_e/A_c in Lam and Teng (2003a) and ACI 440.2R (2008) is defined as

$$A_e/A_c = \left[1 - \left\{(b/h)(h-2r)^2 + (h/b)(b-2r)^2\right\}/\left\{3\left(bh - (4-\pi)r^2\right)\right\} - \rho_g\right]/\left[1-\rho_g\right]$$

This work is devoted to investigating the fundamental Poisson effect in FRP-confined square plain concrete columns made from stone, brick, recycled stone and recycled brick aggregates. Unconfined concrete columns have been tested as primary control specimens and confined stone aggregate concrete columns as secondary control specimens to experimentally clarify the effect of the dilation property on the generation of active confinement with FRP wraps. Single-ply CFRP (carbon-FRP) and GFRP (glass-FRP) wraps were used to offer different passive confining pressures in FRP-confined concretes. The DICT was used to measure the dilation histories of the test pieces at the failure location due to axial load. A methodology has been described to establish a correlation between the dilation history and loading history. $k_1 k_{s1}$ and $k_2 k_{s2}$ are

estimated for concretes of brick and recycled aggregates and compared with those obtained for stone aggregate concrete. The measured quantities were used to predict the confined compressive strengths using available analytical models, and the values were compared with experimental results. In addition, published test data on similar columns of stone aggregate concretes were compared with the current experimental results.

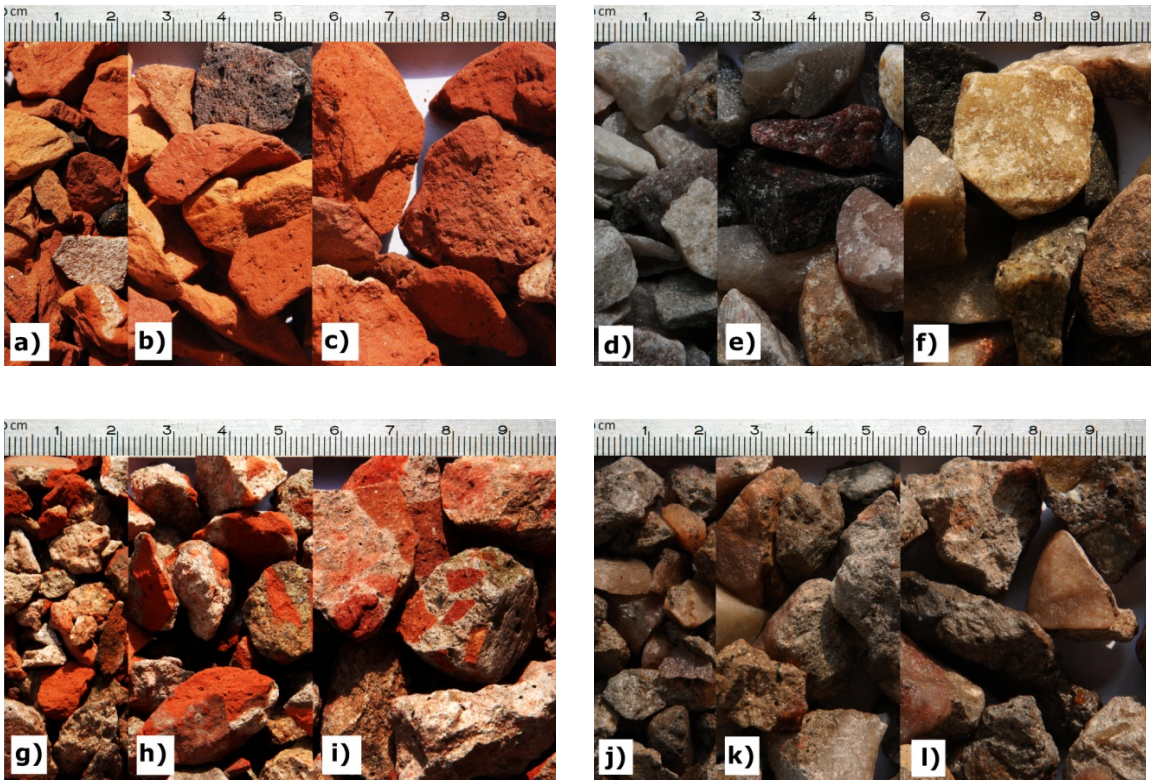

Fig. 3. Types of coarse aggregates used in the research (a), (b), (c) are brick aggregates, (d), (e), (f) are stone aggregates, (g), (h), (i) are recycled brick aggregates and (j), (k), (l) are recycled stone aggregates. Here, (a), (d), (g), (j) aggregates are of 12 mm passing and 6.3 mm retained; (b), (e), (h), (k) are of 19 mm passing and 12 mm retained, and (c), (f), (i), (l) are of 25 mm passing and 19 mm retained. Images by A.F.M.S. Amin.

EXPERIMENTAL DETAILS

Casting and Curing Plain Concrete Columns

Close-up photographs of the four coarse aggregate types that were the subject of the investigation reported in this paper are shown in Figure 3, and Table 2 summarizes their engineering properties. In the figure, mortar is seen to be attached to the parent aggregates in the recycled aggregates. These result in a higher porosity and lower unit weight. The increases in absorption capacities and decreases in the resulting densities, as shown in Table 2, can be explained by considering the presence of adhered mortar. Los Angeles Abrasion (LAA) values are logically seen to be generally higher in brick and recycled aggregates than in stone aggregates. Concretes in old building columns that warrant strengthening are expected to be weak. To replicate such a scenario in the present test program, the authors chose an arbitrary mix design ratio that yielded a target strength between 22-33 MPa, as per ASTM C39/C39M-05.

River bed sand with a bulk specific gravity (saturated surface dry) of 2.58, a bulk specific gravity (oven dry) of 2.54, a bulk unit weight (saturated surface dry) of 1520 kg/m^3 and a fineness modulus of 2.62 was used. The water/cement ratio was maintained at 0.5, and the slump was maintained between 25 and 37 mm. To prepare test specimens meeting such criteria, special customized steel square molds with rounded corners (25 mm corner radius, r) were used to cast the columns. Table 3 shows the IDs of 60 cast specimens and their dimensions. These IDs are cited throughout this paper. All concretes were mixed in a mixer machine, and a poker vibrator was used for compaction. The cast specimens were kept in the molds for 24 h and then removed from the mold and submerged in lime water to cure for 28 days.

Table 2: Properties of coarse aggregates, mix proportions and ultimate strengths of concretes

CA ID	Coarse aggregate				Concrete	
	Unit wt. kg/m^3	Absorption capacity (%)	LAA value (%)	Aggregate sizes (w/w)	Mix proportion (w/w)	f'_c MPa
B	936	14.4	38.0	19 mm-25 mm: 12 mm-19 mm: 6 mm-12 mm 1.24:1.67:1	1:2:4	22
S	1568	0.80	29.5			29
RB	1000	12.40	40.8			33
RS	1223	5.80	38.1			23

CA: Coarse aggregate; LAA: Los Angeles Abrasion

Table 3: Specimen description and sample ID

Specimen ID	Aggregate type	Confinement type	Size (W x B x H) [No. of specimens]
BSCON	Brick (B)	Unconfined	100 x 100 x 200 [2] **150 x 150 x 300 [2]** 200 x 200 x 400 [1] (for each of the Specimens IDs) Total: 60
BSCFRP		CFRP wrap	
BSGFRP		GFRP wrap	
SSCON	Stone (S)	Unconfined	
SSCFRP		CFRP wrap	
SSGFRP		GFRP wrap	
RBSCON	Recycled brick (RB)	Unconfined	
RBSCFRP		CFRP wrap	
RBSGFRP		GFRP wrap	
RSSCON	Recycled stone (RS)	Unconfined	
RSSCFRP		CFRP wrap	
RSSGFRP		GFRP wrap	

W: Width, B: Breadth, H: Height in mm

Surface Preparation and Installation of FRP Confinement

Table 4 shows the engineering properties of the CFRP and GFRP fabric used to confine the specimens. FRP sheets were pasted on the concrete columns, keeping the fiber direction aligned along the hoop direction. The concrete surfaces were dried, cleaned and also made free from surface irregularities before priming. The wraps were installed on the primed surfaces using epoxy-based adhesives as per the manufacturers' specifications. All square column specimens had 25% lapping of FRP-wrap around the perimeter; thus, one of the four sides of the short

column had two layers of wrap. The specimens were tested for compression capacity 7 days following the FRP installation.

Table 4: Engineering properties of CFRP and GFRP wraps (ASTM D 3039 2000)

CFRP wrap	Properties	
Tensile strength, f_{frp}	4,900	MPa
Tensile modulus, E_{frp}	230	GPa
Ultimate elongation, ε_{frp}	1.80	%
Thickness, t_{frp}	0.117	mm
GFRP wrap		
Tensile strength f_{frp}	2,300	MPa
Tensile modulus, E_{frp}	76	GPa
Ultimate elongation, ε_{frp}	2.80	%
Thickness, t_{frp}	0.376	mm

Test Setup, Testing and Data Acquisition

All 60 short concrete column specimens were tested under uniaxial compression at a constant rate of 0.21 MPa/s until failure in a 2,000 kN computer-controlled universal testing machine in accordance with ASTM C39/C39M-05. The vertical displacement and axial load were recorded from the load cell. Unconfined and confined columns of a particular size were tested on the same day to achieve uniformity in the strength of the concrete due to ageing. All tests were completed within 3 consecutive days.

To measure the lateral strain ε_{lD} due to dilation of the column at the failure location, lateral displacements were measured using the DICT by analyzing the image histories obtained from a high definition video camera (Figures 4a). To minimize the interference of lapping on the lateral strain measurement, the side opposite to the lap was turned to the camera (see also Figure 6a). *Scion Image 4.0.2* was used to take linear measurements from captured frame-by-frame still images from HD video footage (60 frames per second). The total vertical displacement (and thus axial strain) history due to axial load and lateral dilation (lateral strain) history of the columns at the failure location were measured in this manner. The measurements are taken by using a customized simultaneous data acquisition system and three level correlations (Figure 4b). To synchronize the time history between two physically independent measurement systems, e.g., the DICT and load cell of the test machine, the peak load recorded at the load cell and the start of failure process recorded by the video camera were taken as a unique event occurring at a specific time. The locations where the failures were initiated varied, as usual. In this process, the lateral strain, the Poisson effect and the confinement due to the dilation of the concretes of different aggregates were synthesized, measured and plotted. The axial strain was also estimated from the DICT data and compared with the load cell displacement records. The axial stress-axial strain and axial stress-lateral strain histories/responses were also plotted using these data.

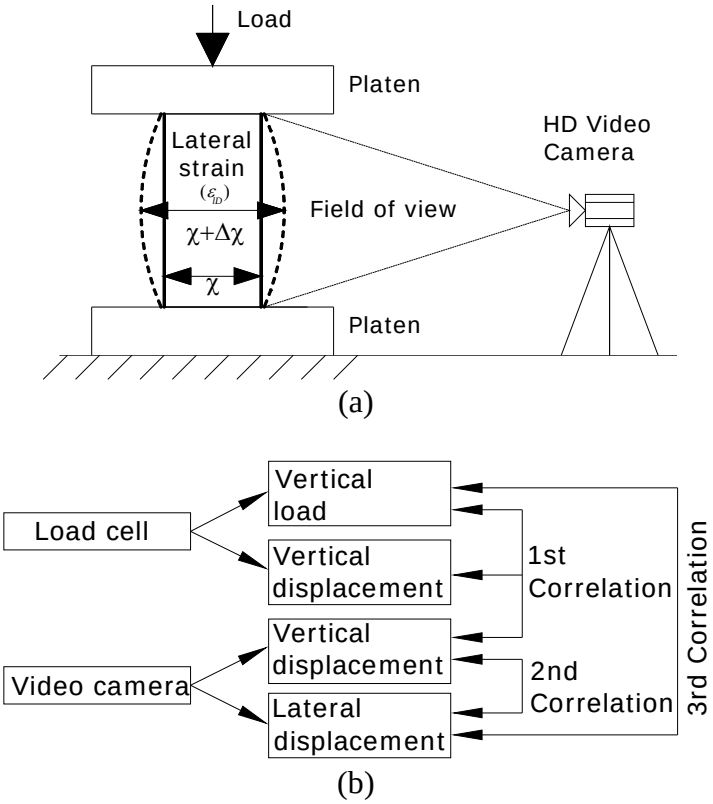

Fig. 4. DICT to measure lateral strain. (a) Layout of the test apparatus (b) Data acquisition scheme. Lateral strain, $\varepsilon_{lD}\ (=\Delta\chi/\chi)$, is taken as an indirect measure of the dilation effect, where χ is the initial width of the specimen and $\Delta\chi$ is the increase in width due to dilation.

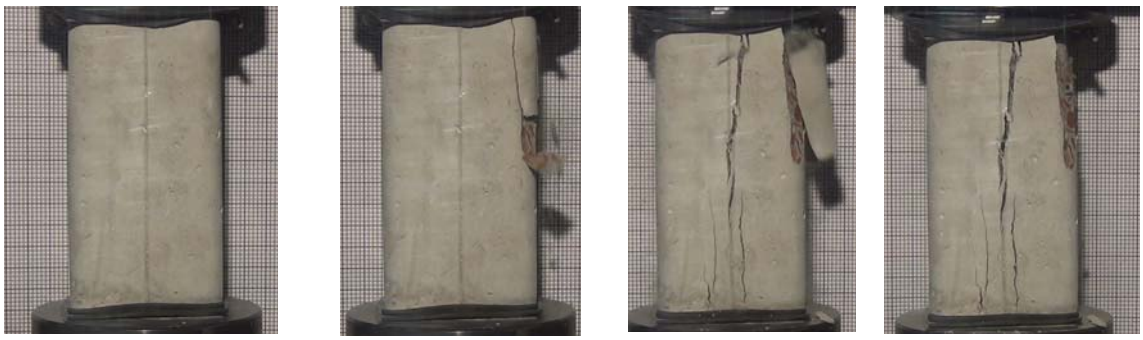

(a) (b) (c) (d)

Fig. 5. Progressive failure of brick aggregate concrete control column (150 mm x 150 mm x 300 mm) under axial compression captured from high-definition video footage. Locations of the captured still image frames in the HD footage: (a) 1 min : 53 sec : 20/60 frame, (b) 1 min : 53 sec : 30/60 frame, (c) 1 min : 54 sec : 37/60 frame, (d) 1 min : 55 sec : 00/60 frame. Images by A.F.M.S. Amin.

Figures 5-6 show the progressive failure of unconfined and CFRP-confined brick aggregate concrete columns at the ultimate load. The failure process in the unconfined column (Figure 5) begins at the corner, where the stress concentration theoretically occurs (Figure 2). Figure 6 illustrates that the failure of the confined column is rapid. Figure 7 shows the typical failure

patterns in FRP-confined columns. Columns failed either due to the rupture of the wrap or the failure of the lap. The unpredictable shifts of failure locations can be clearly observed. However, the processing of HD recorded video footage facilitated the measurement of the dilation at the location where the rupture process was initiated. Measurements were taken at three locations close to the failure location (Figures 5-6), and the average of three measurements was reported. The confining pressure in the FRP due to the dilation of the concrete was calculated using Equation 3.

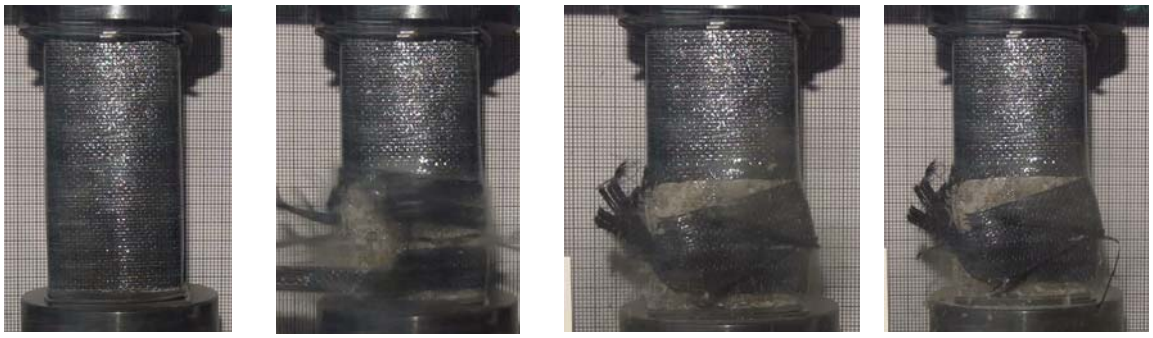

(a) (b) (c) (d)

Fig. 6. Progressive failure of a brick aggregate concrete CFRP-confined column (150 mm x 150 mm x 300 mm) under axial compression captured from high-definition video footage. The side opposite to the lap is facing the camera. Locations of the captured still image frames in the HD footage: (a) 2 min : 13 sec : 58/60 frame, (b) 2 min : 14 sec : 01/60 frame, (c) 2 min : 14 sec : 10/60 frame, (d) 2 min : 14 sec : 18/60 frame. Images by A.F.M.S. Amin.

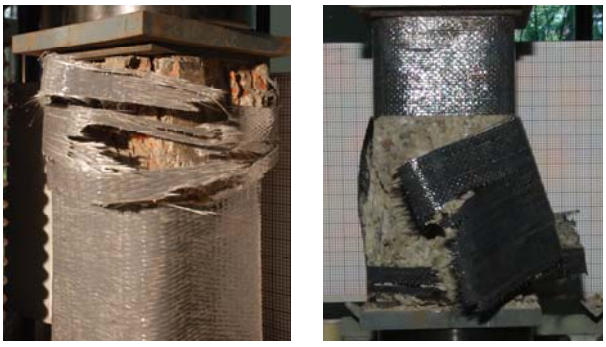

(a) (b)

Fig. 7. Failure patterns of FRP-confined 200 mm x 200 mm x 400 mm columns. After the end of the tests, the specimens were rotated to get the best view of the failure location. (a) GFRP rupture in confined brick aggregate concrete column, (b) CFRP rapture in confined recycled stone aggregate concrete column. Images by A.F.M.S. Amin.

RESULTS AND DISCUSSION

The measurements obtained from 60 test specimens are reported in this section. For brevity, the stress-strain responses from a set of 150 mm x 150 mm x 300 mm specimens (Table 3, column 4, marked in bold) are presented in detail to explain the pertinent findings, and the other results are available elsewhere (Islam 2011 and Choudhury 2012). However, in evaluating the confinement

effectiveness coefficient (k_1k_{s1}) and strain enhancement coefficient (k_2k_{s2}), the entire test result database was considered. All stresses and strains were calculated by dividing the measured loads and displacements by the initial areas and lengths, respectively.

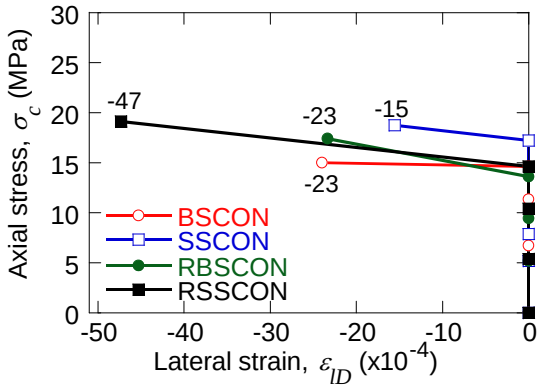

(a)

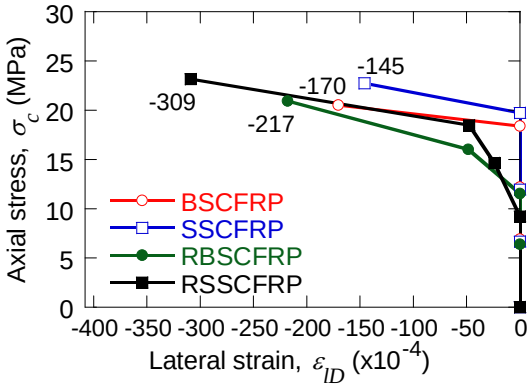

(b)

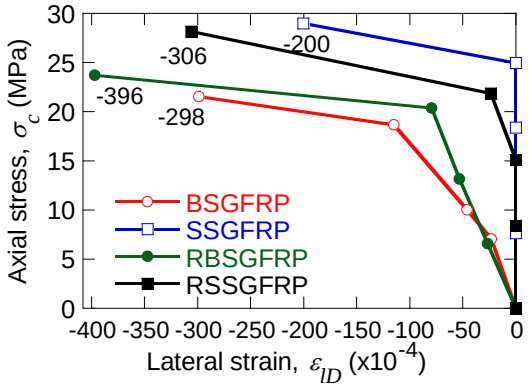

(c)

Fig. 8. Dilation effects in concrete columns of different coarse aggregates. (a) Unconfined column, (b) CFRP-confined column, (c) GRFP-confined column. Numbers in the plot are measured lateral strain (x10^{-4}) values, ε_{lD} .

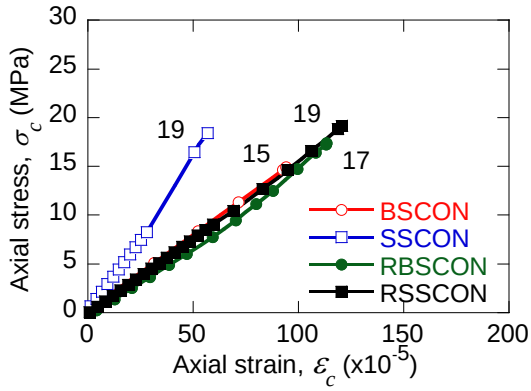

(a)

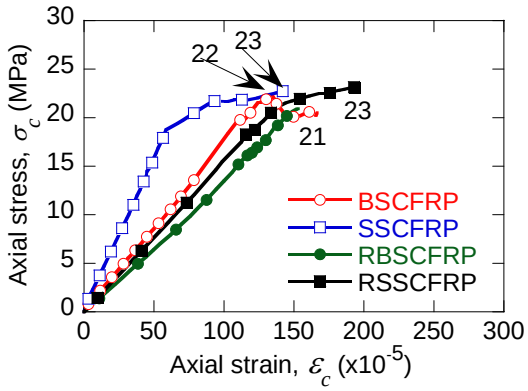

(b)

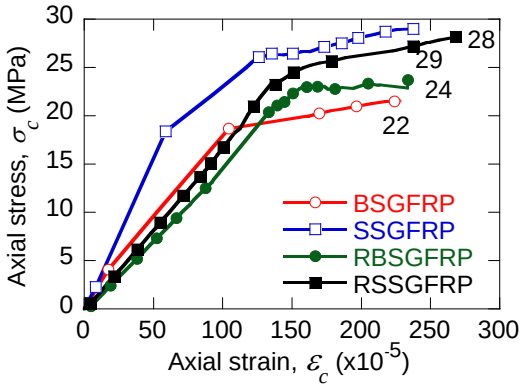

(c)

Fig. 9. Axial stress-axial strain responses of concrete columns of different aggregates. (a) Unconfined columns; (b) CFRP-confined columns; (c) GFRP-confined columns. Numbers in the plot are peak axial stresses in MPa, e.g., f'_{co} in (a) and f'_{cc} in (b) and (c).

Lateral Strain, ε_{lD}, in Unconfined and FRP-confined Concretes

Figure 8 presents the lateral strains due to dilation effects measured in concrete columns of different aggregates. A comparison of the plotted axial stress-lateral strain responses illustrates

that the dilation is significantly higher in concretes made of brick and recycled aggregates, which have a lower unit weight and higher absorption capacity (Table 2). These aggregates also typically have a lower modulus of elasticity than stone aggregate concrete (Figure 1). Compared to the CFRP wrap used in this work, GFRP wrap with larger ultimate elongation (ε_{frp}) and thickness (t_{frp}) properties (Table 4) has yielded significantly better performance in confining concretes of all aggregate types, as its lower tensile modulus (E_{frp}) may enable the accommodation of greater dilation under loads.

Axial Capacity Enhancements in Concretes of Different Coarse Aggregates

Figure 9 presents the axial stress-axial strain responses of unconfined and confined concrete columns made with different aggregates. The unconfined concrete column (Figure 9a) of a stone aggregate, similar to those widely investigated in previous studies and conventionally used in construction, exhibited higher axial stiffness than columns made of brick and recycled aggregate concretes. This is in striking conformity with independent observations (see also Figure 1, the respective modulus of elasticity values in the figure caption and related discussions) of other research groups (Mohammed et al. 2007; Mohammed et al. 2014; Zhao et al. 2014). The confined concrete columns (Figure 9b,c) showed a similar trend, but they sustained higher ultimate loads and axial strains, indicative of greater ductility. The performance of GFRP-confined columns in axial capacity enhancement was superior to CFRP-confined columns, likely due to differences in their material properties (Table 4). The measurements of ε_{lD} and the axial capacity enhancements for stone aggregate concrete are further synthesized and discussed in the following subsections to demonstrate their conformity with other published results regarding similar aggregate types and their remarkable dissimilarity from those of brick and recycled aggregate concretes.

Estimation of the Confined Concrete Model Parameters

The unconfined compressive strength (f'_{co}), confined compressive strength (f'_{cc}), ultimate lateral strain at rupture of an unconfined column (ε_{lo}), ultimate lateral strain at rupture of a confined column ($\varepsilon_{l,rup}$), ultimate compressive strain of an unconfined column (ε_{co}), and confined compressive strain (ε_{cu}) measured from the dataset of 60 specimens (Table 3, see also Figure 2) are considered here together to estimate the $k_1 k_{s1}$ and $k_2 k_{s2}$ parameters of Equations 1-2. The confining pressure, f_{lD}, was calculated using Equation 3. The f'_{cc}/f'_{co} vs. f_{lD}/f'_{co} and $\varepsilon_{cu}/\varepsilon_{co}$ vs. f_{lD}/f'_{co} relations are plotted in Figures 10 and 11, respectively, for each of the aggregates. Linear fits were obtained employing a least-squares technique in *KaleidaGraph 4.1*. A single fit for the data points was obtained from three different specimen sizes (Table 3), ignoring the size effect. The Pearson's R values are shown in the figures. The value of υ (Equation 3) is taken as 1.00 for the specimens considered in this test.

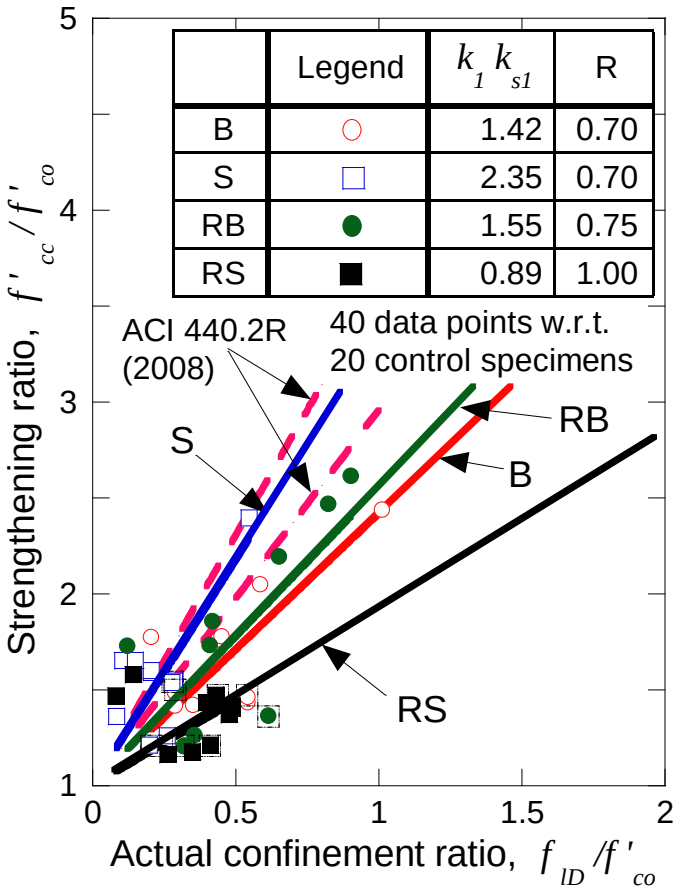

Fig. 10. Strengthening ratio vs. actual confinement ratio plots for CFRP-confined and GFRP-confined columns. Data points inside the dotted box are derived from the dataset presented in Figures 8 and 9.

A closer look at the fits in Figure 10 shows a relatively higher value of $k_1 k_{s1}$ for the stone aggregate concrete than the brick and recycled aggregate concretes. To further justify the experimental observations, the natural limits of variation of $k_1 k_{s1}$ suggested in ACI 440.2R (2008) for stone aggregate concrete (Table 1) for the test specimen sizes were also plotted (see Table 1 and its footnote for the corresponding equations). ACI 440.2R (2008) suggests values that lie between 1.95 and 2.61, in agreement with the result of this study, 2.35, and clearly different from the results obtained for brick and recycled aggregate concretes. The column of recycled stone aggregate concrete yielded the lowest value of 0.89. This fundamental observation indicates that to generate the same amount of hoop stress, and thus the stress in the FRP confinement, stone aggregate concrete requires significantly greater axial compression than concretes having lower $k_1 k_{s1}$ values. A further look at Figure 11 illustrates the well noted different behavior of brick and recycled aggregate concretes than stone aggregate concrete. To compare the experimental observations, the limits of variation of $k_2 k_{s2}$ suggested in ACI 440.2R (2008) for stone aggregate concrete (see Table 1 and its footnote for the corresponding equations) for the test specimen sizes were also plotted. ACI 440.2R (2008) suggests values between 11.2 and 18.2, close to the test result for stone aggregate concrete, 6.90, but remarkably different from the brick and recycled aggregate concretes. The different behavior displayed by the former type of aggregate implies that to attain a particular degree of dilation, the stone

aggregate concrete requires the generation of hoop strains in the FRP wrap at a greater axial strain than the brick aggregate and recycled aggregate concretes. The lower modulus of elasticity values of the brick and recycled aggregates (Figure 1), possibly resulting from their lower unit weights, higher absorption capacities and higher LAA values due to porosity (Table 2), might be the reason behind the unique k_1k_{s1} and k_2k_{s2} properties in these concretes. The trend of variation in the results for the dilatable aggregates i.e. brick and recycled aggregates presented in Figures 8-11 may be attributed to the effect of specimen size. In Figures 8-9, the results from only one specimen size were plotted, whereas in developing the best fits (Figures 10-11), all specimen sizes were considered together.

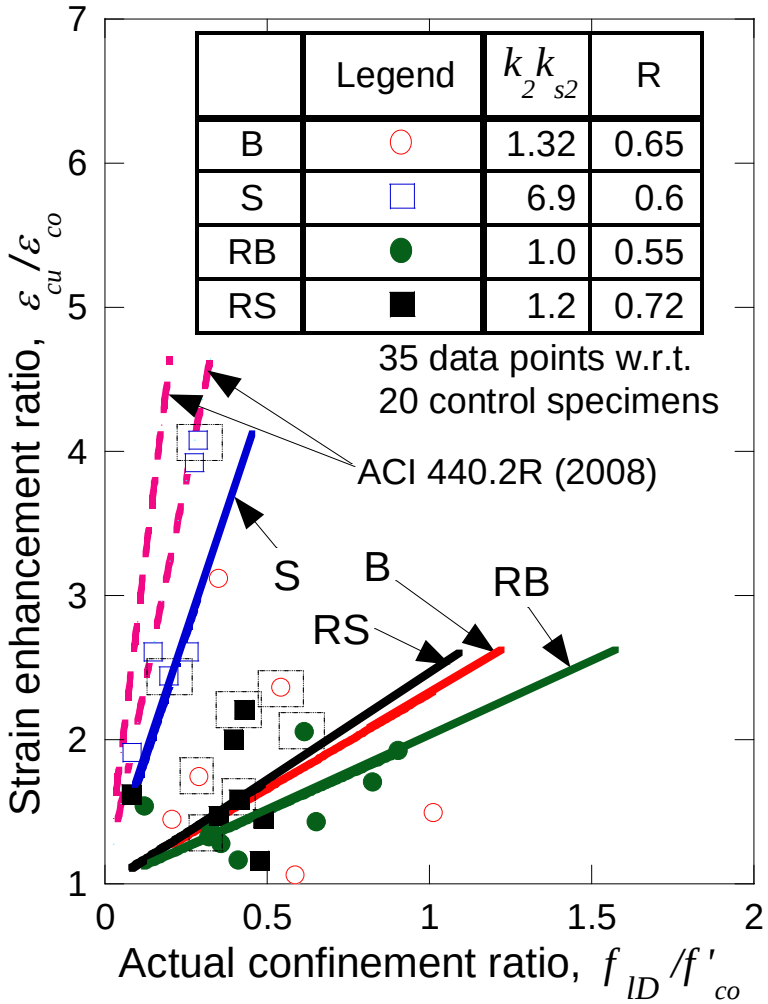

Fig. 11. Strain enhancement ratio vs. actual confinement ratio plots for CFRP-confined and GFRP-confined columns. Data points inside the dotted box are derived from the dataset presented in Figures 8 and 9.

Comparison between Different Models

The k_1k_{s1} and k_2k_{s2} parameters evaluated for concretes with different aggregates are compared in Table 5, with eight available models summarized in Table 1. To do this, the values of

$f'_{cc(\exp)}/f'_{cc(model)}$ and $\varepsilon_{cu(\exp)}/\varepsilon_{cu(model)}$ for each of the models listed in Table 1 have been calculated for the materials and specimens reported in this paper.

Table 5: Comparative performance of different published models and proposed model in predicting the authors' test results.

	Confinement models	$f'_{cc(\exp)}/f'_{cc(model)}$		$\varepsilon_{cu(\exp)}/\varepsilon_{cu(model)}$	
		Average*	COV	Average*	COV
Brick	Authors' Model	1.03	0.22	1.11	0.44
	Wu and Wang (2009)	0.67	0.21	-	-
	ACI 440.2R (2008)	0.85	0.3	0.27	0.6
	Youssef et al. (2007)	1.41	0.21	0.42	0.57
	Kumutha et al. (2007)	1.19	0.18	-	-
	Al-Salloum (2007)	0.67	0.43	-	-
	Lam and Teng (2003a)	0.83	0.31	0.3	0.59
	ACI 440.2R (2002)	0.65	0.21	0.19	0.14
	Shehata et al. (2002)	1.22	0.18	0.27	0.52
Stone	Authors' Model	1.09	0.23	0.9	0.45
	Wu and Wang (2009)	1.31	0.18	-	-
	ACI 440.2R (2008)	1.09	0.22	0.57	0.51
	Youssef et al. (2007)	1.33	0.16	0.82	0.47
	Kumutha et al. (2007)	1.36	0.2	-	-
	Al-Salloum (2007)	0.9	0.27	-	-
	Lam and Teng (2003a)	1.08	0.22	0.64	0.5
	ACI 440.2R (2002)	0.62	0.18	0.16	0.17
	Shehata et al. (2002)	1.38	0.2	0.59	0.46
RB	Authors' Model	0.94	0.25	1.07	0.35
	Wu and Wang (2009)	1.05	0.24	-	-
	ACI 440.2R (2008)	0.79	0.32	0.25	0.71
	Youssef et al. (2007)	1.36	0.15	0.38	0.63
	Kumutha et al. (2007)	1.12	0.22	-	-
	Al-Salloum (2007)	0.62	0.49	-	-
	Lam and Teng (2003a)	0.77	0.33	0.28	0.68
	ACI 440.2R (2002)	0.63	0.16	0.17	0.24
	Shehata et al. (2002)	1.15	0.22	0.25	0.59
RS	Authors' Model	1.16	0.14	1.24	0.5
	Wu and Wang (2009)	1.09	0.17	-	-
	ACI 440.2R (2008)	0.86	0.26	0.4	0.85
	Youssef et al. (2007)	1.32	0.12	0.58	0.74
	Kumutha et al. (2007)	1.15	0.14	-	-
	Al-Salloum (2007)	0.69	0.41	-	-
	Lam and Teng (2003a)	0.84	0.27	0.45	0.82
	ACI 440.2R (2002)	0.62	0.13	0.18	0.24
	Shehata et al. (2002)	1.17	0.13	0.41	0.78

Average of the experimental data points presented in Figures 10 and 11.

The values of f'_{co} for the respective aggregates were taken from the experimental data. The average values obtained for each of the specimen groups (Table 3) along with coefficient of

variation (COV) are listed. Better fits, as indicated by average $f'_{cc(\exp)}/f'_{cc(model)}$ (and $\varepsilon_{cu(\exp)}/\varepsilon_{cu(model)}$) values closer to 1.00 and lower COVs, are generally seen for calculations using the parameters from Figures 10-11 and Equations 1-2 rather than those proposed by other authors. The divergences appear to be more significant in the prediction of $\varepsilon_{cu(\exp)}/\varepsilon_{cu(model)}$. Nevertheless, the axial stress predictions calculated using different models well support (within 10% accuracy) the connotations of Lam and Teng (2003a) and ACI 440.2R (2008) for stone aggregate concrete and those of Wu and Wang (2009) for recycled aggregates. The model proposed by Kumutha et al. (2007) performed within 15% accuracy for recycled aggregates. However, none of the eight models could reproduce a logical result within 15% accuracy for the brick aggregate concrete. The remarkable overprediction of the model of ACI 440.2R (2002) is also well noted for all aggregate types. The axial strains measured in the current study are significantly lower than those predicted by the tabulated models, whereas the measured lateral strains, ε_{lD}, in the brick and recycled aggregate concretes depicted in Figure 8, 10 and 11 are significantly higher because of the generation of additional hoop strain, ε_r, caused by the FRP confinement. All four aggregates, even the stone aggregate, studied in this work, are of Bangladeshi origin and are softer in character with comparatively lower modulus of elasticity (see the caption of Figure 1 for the modulus of elasticity values) and larger LAA values than granite and other igneous rocks used elsewhere in the world. This might have led to some differences in the comparison. However, the apparent modulus of elasticity obtained for unconfined concrete in this work are in conformity with those obtained independently in Mohammed et al. (2007), Figure 1 for similar aggregate types.

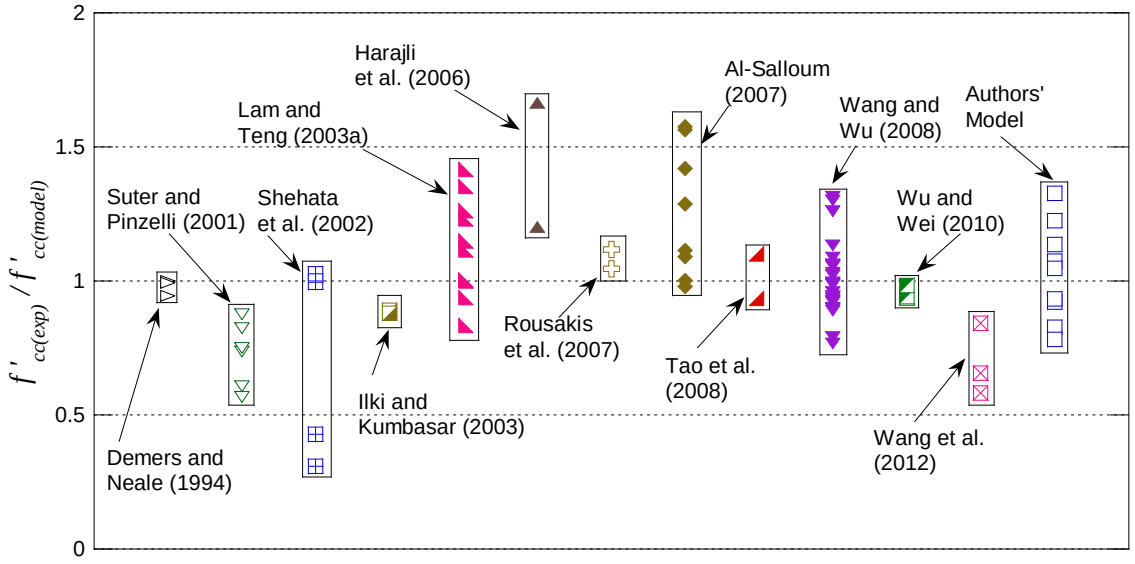

Fig. 12. Representation of confined compressive strengths against different published test data sets on stone aggregate concrete square columns by Authors' model using the k_1k_{s1} coefficient of Equation 1 assessed in Figure 10. $f'_{cc(\exp)}$ are the test data taken from different published studies, and $f'_{cc(model)}$ are respective predicted confined compressive strengths obtained using the authors' model.

The representation of f'_{cc} via the authors' model using the $k_1 k_{s1}$ parameters estimated from the test results reported here (Figure 10) has been checked against the published test data obtained for similar specimens by twelve other research groups, as shown in Figure 12. The results of five test datasets (Demers and Neale 1994; Ilki and Kumbasar 2003; Rousakis et al. 2007; Tao et al. 2008; Wu and Wei 2010) are in close conformity, indicating a general coherence in the $k_1 k_{s1}$ parameter estimates for stone aggregate concrete.

These observed differences between stone aggregate concrete and dilatable aggregate concretes may have an impact on the $P-M$ interaction diagram, as confined concrete model parameters are often used to plot $P-M$ diagrams. A set of equations are provided in Appendix D of ACI 440.2R (2008) to calculate the resultant force in the compression zone in a standard $P-M$ interaction diagram. In the basic relations (Equations 1-2), parameter $k_1 k_{s1}$ governs the value of P_n, the nominal axial capacity. The values of P_n and M_n at other critical points also depend on both the $k_1 k_{s1}$ and $k_2 k_{s2}$ parameters. Thus, the measurements provided in this essay may be useful as indicative values for the construction of $P-M$ interaction diagrams for a range of aggregates that exhibit considerable dilation.

CONCLUSIONS

1. The fundamental dilation property due to axial compression is measured with a DICT in plain concrete square columns produced using new crushed stone and new crushed brick, as well as recycled brick and recycled stone from old concretes, as coarse aggregates. The measurements were taken both on unconfined and FRP-confined specimens.

2. The measurements show a distinctly higher lateral strain in the concrete columns produced from the brick and recycled aggregates than in those produced from stone aggregates due to the former's dilation property.

3. The higher lateral strain measured in specimens of dilatable concretes motivated the authors to estimate the fundamental parameters of the compressive strength model and ultimate axial strain model of confined concretes for each of the aggregates. The distinctly lower parameter values for FRP-confined brick and recycled aggregate concrete columns suggest that the confinement induced by the FRP wraps resulted in overstressing at a lower axial strain due to the larger dilation effect. This led to a lower axial capacity enhancement in concretes of these aggregates.

4. The experimental results and the performance of the confinement models derived from the test data on the stone, brick and recycled aggregate concrete columns reported in this essay have been checked against the models and test datasets available in the published literature for stone aggregate concrete columns of similar geometry. The performance evaluation demonstrates a close conformity for the stone aggregate concrete columns but justifies the necessity of paying special attention in designing confinements for columns of dilatable aggregates.

Acknowledgement
The authors are grateful to the members and staff of the Concrete Laboratory and Structural Mechanics Laboratory, Department of Civil Engineering, Bangladesh University of Engineering and Technology for their support and cooperation in conducting the tests. The authors gratefully acknowledge the kind cooperation extended by the LaMaCo System Sdn Bhd, Malaysia in providing samples of the fiber-reinforced polymer wraps used in this investigation. The authors also sincerely acknowledge the funding and technical assistance provided by the Committee for Advanced Studies and Research, BUET, Dhaka, Bangladesh and M/S Aziz & Company Limited, Dhaka, Bangladesh.

REFERENCES

Abdelrahman, K. and El-Hacha, R. (2014a). "Cost and ductility effectiveness of concrete columns strengthened with CFRP and SFRP sheets." Polymers, 6(5), 1381-1402.

Abdelrahman, K. and El-Hacha, R. (2014b)."State-of-the-art review on FRP strengthened concrete columns" Concrete solutions, 253-260.

ACI 440.2R-02. (2002). "Guide for the design and construction of externally bonded FRP systems for strengthening concrete structures." American Concrete Institute, Farmington Hills, MI.

ACI 440.2R-08. (2008). "Guide for the design and construction of externally bonded FRP systems for strengthening concrete structures." American Concrete Institute, Farmington Hills, MI.

Akhtaruzzaman, A. A. and Hasnat, A. (1983). "Properties of concrete using crushed brick as aggregate." Concrete International, 5(2), 58-63.

Al-Salloum, Y. A. (2007). "Influence of edge sharpness on the strength of square concrete columns confined with FRP composite laminates." Composites Part B: Engineering, 38(5), 640-650.

ASTM C39/C39M-05. (2005). "Standard Test Method for Compressive Strength of Cylindrical Concrete Specimens." ASTM International, West Conshohocken, PA, 2014.

ASTM D 3039/D 3039M-00. (2000). "Standard Test Method for Tensile Properties of Polymer Matrix Composite Materials." ASTM International, West Conshohocken, PA, 2014.

Buck, A.D. (1977). "Recycled concrete as a source of aggregate." ACI Journal, 74(5), 212-219.

Cachim, P.B. (2009). "Mechanical properties of brick aggregate concrete." Construction and Building Materials, 23(3), 1292-1297.

Choudhury, M.S.I., (2012). "Confinement effect of fiber reinforced polymer wraps on circular and square concrete columns." M.Sc. Engg. Thesis, Department of Civil Engineering, Bangladesh University of Engineering and Technology, Dhaka, Bangladesh.

Debieb, F. and Kenai, S. (2008)."The use of coarse and fine crushed bricks as aggregate in concrete." Construction and Building Materials, 22(5), 886-893.

Demers, M., and Neale, K.W. (1994). "Strengthening of Concrete Columns with Unidirectional Composite Sheets." In: Mufti, A. A., Bakht, B., and Jaeger, L.G. (eds), Development in Short and Medium Span Bridge Engineering '94, Proceedings of the Fourth International Conference on Short and Medium Span Bridges, 895–905, Canadian Society for Civil Engineering, Montreal, Canada.

El-Hacha, R and Abdelrahman, K. (2013). "Slenderness effect of circular concrete specimens confined with SFRP sheets." Composites Part B: Engineering, 44(1), 152–166.

Frondistou-Yannas, S. (1977). "Waste concrete as aggregate for new concrete." ACI Journal Proceedings, 74(8), 373-376.

Girgin, Z. C. (2009). "Modified failure criterion to predict ultimate strength of circular columns confined by different materials." ACI Structural Journal, 106(6), 800-809.

Hansen, T.C. andNarud, H. (1983)."Strength of recycled concrete made from crushed concrete coarse aggregate." Concrete International, 5(1), 79-83.

Harajli, M. H., Hantouche, E., and Soudki, K. (2006). "Stress-strain model for fiber-reinforced polymer jacketed concrete columns." ACI Structural Journal, 103(5), 672–682.

Ilki, A., and Kumbasar, N. (2003). “Compressive behaviour of carbon fibre composite jacketed concrete with circular and non-circular cross-sections.” Journal of Earthquake Engineering, 7(3), 381–406.

Islam, M.M., (2011). “Interaction diagrams for square concrete columns confined with fiber reinforced polymer wraps.” M.Sc. Engg. Thesis, Department of Civil Engineering, Bangladesh University of Engineering and Technology, Dhaka, Bangladesh.

Islam, M.M., Choudhury, M.S.I., Abdulla, M., and Amin, A.F.M.S. (2011). “Confinement effect of fiber reinforced polymer wraps in circular and square concrete columns.” 4th Annual Paper Meet and 1st Civil Engineering Congress, The Institution of Engineers (IEB), Dhaka, Bangladesh, 359–362.

Issa, M. A., Alrousan, R. Z., and Issa, M. A. (2009). “Experimental and parametric study of circular short columns confined with CFRP composites.” Journal of Composites for Construction, 13(2), 135-147.

KaleidaGraph 4.1 [Computer software]. Synergy Software, U.S. Headquarters, 2457 Perkiomen Ave., Reading, PA 19606.

Khalaf, F.M. (2006). “Using crushed clay brick as coarse aggregate in concrete.” Journal of Materials in Civil Engineering, 18(4), 518-526.

Khalaf, F.M. and DeVenny, A.S.(2005). “Properties of new and recycled clay brick aggregates for use in concrete.” Journal of Materials in Civil Engineering, 17(4), 456-464.

Kumutha, R., Vaidyanathan, R., and Palanichamy, M. S. (2007). “Behaviour of reinforced concrete rectangular columns strengthened using GFRP.” Cement and Concrete Composites, 29(8), 609-615.

Lam, L. and Teng, J.G. (2003a). “Design-oriented stress–strain model for FRP-confined concrete in rectangular columns.” Journal of Reinforced Plastics and Composites, 22(13), 1149-1186.

Lam, L. and Teng, J.G. (2003b). “Design-oriented stress–strain model for FRP-confined concrete.” Construction and Building Materials, 17(6-7), 471–489.

Lim, J. and Ozbakkaloglu, T. (2014). “Confinement Model for FRP-Confined High-Strength Concrete.” Journal of Composites for Construction, 18(4), 04013058.

Luca, A. D., Nardone, F., Matta, F., Nanni, A., Lignola, G. P., and Prota, A. (2011). “Structural evaluation of full scale FRP-confined reinforced concrete columns.” Journal of Composites for Construction, 15(1), 112-123.

Mansur, M.A., Wee, T.H., and Cheran, L.S. (1999).“Crushed bricks as coarse aggregate for concrete.” ACI Materials Journal, 96(4), 478-484.

Miller, D. (2013). Last nightshift in Savar: The story of the spectrum sweater factory collapse. McNidder and Grace Limited, 4 Chapel Lane, Alnwick, Northumberland, NE66 1XT, United Kingdom.

Mirmiran, A. and Shahawy, M. (1997a). “Dilation characteristics of confined concrete.”Mechanics of Cohesive-Frictional Materials, 2(3), 237–249.

Mirmiran, A. and Shahawy, M. (1997b).“Behavior of concrete columns confined by fiber composites.” Journal of Structural Engineering, 123(5), 583–590.

Mirmiran, A., Shahawy, M., Samaan, M., Echary, H. E., Mastrapa, J. C., and Pico, O. (1998). “Effect of column parameters on FRP-confined concrete.” Journal of Composites for Construction, 2(4), 175-185.

Mohammed, T.U., Awal, M. A., Mahbub, A. A., and Mohammed, R. H., (2007). “Recycling of demolished concrete as coarse aggregate.” Proceedings of the ACBM/ACI International Conference on Advances in Cement Based Materials and Applications to Civil Infrastructure, Editors. Rizwan, S. A. and Ghaffar A., Vol. 2, A-One Publisher, Lahore, Pakistan, 2007, pp. 1077-1090.

Mohammed, T.U., Hasnat, A., Awal, M., and Bosunia, S. (2014). “Recycling of brick aggregate concrete as coarse aggregate.” Journal of Materials in Civil Engineering,10.1061/(ASCE)MT.1943-5533.0001043 , B4014005.

Pessiki, S., Harries, K. A., Kestner, J. T., Sause, R. and Ricles, J. M. (2001). “Axial behavior of reinforced concrete columns confined with FRP jackets.” Journal of Composites for Construction, 5(4), 237-245.

Richart, F. E., Brandtzaeg, A., and Brown, R. L. (1928). “A study of the failure of concrete under combined compressive stresses.” Bulletin 185, University of Illinois Engineering Experimental Station, Champaign, III.

Richart, F. E., Brandtzaeg, A., and Brown, R. L. (1929). “The failure of plain and spirally reinforced concrete in compression.” Bulletin 190, University of Illinois Engineering Experimental Station, Champaign, III.

Rochette, P. and Labossière, P. (2000). “Axial testing of rectangular column models confined with composites.” Journal of Composites for Construction, 4(3), 129-136.

Rousakis, T. C., Karabinis, A. I., and Kiousis, P. D. (2007). “FRP-confined concrete members: Axial compression experiments and plasticity modelling.” Engineering Structures, 29(7), 1343-1353.

Saadatmanesh, H., Ehsani, M. R., Li, M. W. (1994). “Strength and ductility of concrete columns externally reinforced with fiber composite straps.” ACI Structural Journal, 91(4), 434-447.

Scion Image, User Manual, Scion Corporation, Frederick, MD, USA, 2000.

Shahawy, M., Mirmiran, A. and Beitelman, A. (2000).“Test and modeling of carbon-wrapped concrete columns.” Composites: Part B, 31(6), 471–480.

Shehata, I. A. E. M., Carneiro, L. A. V. and Shehata, L. C. D. (2002). “Strength of short concrete columns confined with CFRP sheets.” Materials and Structures, 35(1), 50–58.

Smith, S. T., Kim, J. S. and Zhang, H. (2010). “Behavior and effectiveness of FRP wrap in the confinement of large concrete cylinders.” Journal of Composites for Construction, 14(5), 573-582.

Suter, R., and Pinzelli, R. (2001). “Confinement of concrete columns with FRP sheets.” Proc., 5th Int. Conf. on Fibre Reinforced Plastics for Reinforced Concrete Structures, Univ. of Cambridge, Cambridge, U.K. 793–802.

Tao, Z., Yu, Q., and Zhong, Y. Z. (2008). “Compressive behaviour of CFRP-confined rectangular concrete columns.” Magazine of Concrete Research, 60(10), 735–745.

Teng, J. G., Huang, Y. L., Lam, L. and Ye, L. P. (2007).“Theoretical model for fiber-reinforced polymer-confined concrete.” Journal of Composites for Construction, 11(2), 201-210.

Teng, J.G., Chen, J.F., Smith, S.T., Lam, L. (2002). “FRP: Strengthened RC Structures.” John Wiley and Sons, Inc., England, ISBN: 978-0-471-48706-7.

Toutanji, H., Han, M. Gilbert, J. and Matthys, S. (2010). “Behavior of large scale rectangular columns confined with FRP composites.” Journal of Composites for Construction, 14(1), 62-71.

Wang, L. M., and Wu, Y. F. (2008).“Effect of corner radius on the performance of CFRP-confined square concrete columns: Test.” Engineering Structures, 30(2), 493-505.

Wang, Z. Y., Wang, D. Y., Smith, S. T., and Lu, D. G. (2012). “CFRP confined square RC columns. I: Experimental investigation.” Journal of Composites for Construction, 16(2), 150-160.

Wu, Y. F., and Wei, Y. Y. (2010). “Effect of cross-sectional aspect ratio on the strength of CFRP-confined rectangular concrete columns.” Engineering Structures, 32(1), 32–45.

Wu, Y.F. and Wang, L.M. (2009). “Unified strength model for square and circular concrete columns confined by external jacket.” Journal of Structural Engineering, 135(3), 253-261.

Xiao, J., Li, J. and Zhang, C. (2005).“Mechanical properties of recycled aggregate concrete under uniaxial loading.” Cement and Concrete Research, 35(6), 1187-1194.

Yang, K.,Chung, H. and Ashour A.F. (2008). “Influence of type and replacement level of recycled aggregates on concrete properties.”ACI Materials Journal, 105(3), 289-296.

Yardley, J. (2013). “Report on deadly factory collapse in Bangladesh finds widespread blame.” May 22, 2013, The New York Times.

Youssef, M. N., Feng, Q., and Mosallam, A. S. (2007).“Stress-strain model for concrete confined by FRP composites.” Composites: Part B, 38(5), 614–628.

Zhao, J., Yu, T., and Teng, J. (2014).“Stress-Strain Behavior of FRP-Confined Recycled Aggregate Concrete.” Journal of Composites for Construction,10.1061/(ASCE)CC.1943-5614.0000513 , 04014054.